Electronic properties of single-layer and multilayer transition metal dichalcogenides MX_2 ($M =$ Mo, W and $X =$ S, Se)

Rafael Roldán[1,], Jose A. Silva-Guillén[2,4], M. Pilar López-Sancho[1], Francisco Guinea[1], Emmanuele Cappelluti[3], and Pablo Ordejón[2,4]*

Single- and few-layer transition metal dichalcogenides have recently emerged as a new family of layered crystals with great interest , not only from the fundamental point of view, but also because of their potential application in ul-trathin devices. Here the electronic properties of semiconducting MX_2, where $M =$ Mo or W and $X =$ S or Se, are reviewed. Based on of density functional theory calculations, which include the effect of spin-orbit interaction, the band structure of single-layer, bilayer and bulk compounds is discussed. The band structure of these compounds is highly sensitive to elastic deformations, and it is reviewed how strain engineering can be used to manipulate and tune the electronic and optical properties of those materials. Further, the effect of disorder and imperfections in the lattice structure and their effect on the optical and transport properties of MX_2 is discussed. The superconducting transition in these compounds, which has been observed experimentally, is analyzed, as well as the different mechanisms proposed so far to explain the pairing. Finally, a discussion on the excitonic effects which are present in these systems is included.

1 Introduction

Two-dimensional layered materials are currently being object of great attention due to their physical properties. Single-layer and few-layer graphene have received much attention and bolstered this field of research [1]. Recently, the focus is widening to other two-dimensional materials with interesting structural and electronic properties [2]. Transition metal dichalcogenides (TMD) form a new family of layered materials that can be easily exfoliated and present promising electrical and optical properties [3]. Among these materials, semiconducting TMD are of special interest since the gap present in both

single-layer and multi-layer samples makes them candidates for device applications [4–6].

The band structure of those compounds dramatically changes from single-layer to multi-layer samples, involving a transition from a direct gap for single-layer samples to an indirect gap for multi-layer samples [7], as it has been observed experimentally [8–11], pointing out the important role of interlayer coupling [12]. Furthermore, their electronic properties are highly sensitive to the external conditions such as temperature, pressure or strain. For instance, an insulator/metal transition can be induced under particular conditions [13–25]. This tunability of the gap is very interesting for optoelectronic applications [4].

Other important feature of the TMD is the possibility to control quantum degrees of freedom as the electron spin, the valley pseudospin and layer pseudospin [26]. In fact, the strong spin-orbit interaction in these compounds, and the coupling of the spin, the valley and the layer degrees of freedom opens the possibility to manipulate them for future applications in spintronics and valleytronics devices [27–34]. The spin orbit coupling (SOC) lifts the spin degeneracy of the energy bands in single layer samples due to the abscence of inversion symmetry [35]. By time reversal symmetry the spin splitting in inequivalent valleys must be opposite, leading to the so called spin-valley coupling [31], which have been observed experimentally [27, 29, 32, 33, 36, 37] and have also been studied theoretically [38–43].

* Corresponding author E-mail: rroldan@icmm.csic.es
[1] Instituto de Ciencia de Materiales de Madrid, CSIC, Sor Juana Ines de la Cruz 3, 28049 Cantoblanco, Madrid, Spain
[2] ICN2 - Institut Catala de Nanociencia i Nanotecnologia, Campus UAB, 08193 Bellaterra, Spain
[3] Istituto di Sistemi Complessi, U.O.S. Sapienza, CNR, v. dei Taurini 19, 00185 Roma, Italy
[4] CSIC - Consejo Superior de Investigaciones Ciaentificas, ICN2 Building, 08193 Bellaterra, Spain

Due to the reduced dielectric screening in monolayer and few-layer samples of TMDs, excitonics effects are especially relevant in these compounds. The existence of neutral and charged excitons, as well as their possible manipulation for optoelectronic applications, is attracting a lot of interest from both, experimental [28, 44–46] and theoretical [47–49] points of view.

Similarly as in graphene, metallic behavior can be induced in semiconducting TMD by means of electric field effects or by doping. At high carrier concentrations ($n \sim 10^{14}$ cm^{-2}), and in the presence of high-κ dielectrics, MoS$_2$ becomes superconductor, with a doping-dependent critical temperature T$_c(n)$ which exhibits a *superconducting dome* with a maximum for a certain range of doping n and drops to zero at sufficiently large values of n [50, 51], and whose understanding is focus of a number of recent theoretical works [52–55].

Another topic of current research is the effect of disorder on the optical and electronic properties of TMDs. In particular, the presence of vacancies or adatoms in the samples can modify their mobility, and the importance of short-range disorder is thought as one of the main limitations for the mobility of chemical vapor deposition (CVD) grown single-layer MoS$_2$ [56, 57]. Theoretically, this problem has been studied using *ab initio* methods [58–65], as well as *real space* tight-binding (TB) methods which can simulate realistic samples [66].

The present paper analyzes the electronic properties of the group-VIB MX_2 (where $M = $ Mo, W and $X = $ S, Se). The corresponding band structure for single layer, bilayer and bulk compounds is obtained from density function theory (DFT) calculations, which includes spin-orbit interaction. We discuss the role played by both, the metal and the chalcogen atoms, in the optical and electronic properties of these materials. We review the effects of strain and disorder in the electronic spectrum, as well as the superconducting transition in highly doped samples.

2 Electronic structure

In this section we discuss the main features of the electronic band structure of single-layer, bilayer and bulk TMDs. For this, we will use DFT calculations, including the intrinsic spin-orbit interaction term for all atoms. The crystal structure of single-layer and multilayer MX_2 is schematically shown in Fig. 1. The basic unit block of MX_2 is composed of an inner layer of M atoms on a triangular lattice sandwiched between two layers of X atoms lying on the triangular net of alternating hollow sites. We denote [7] a as the distance between nearest
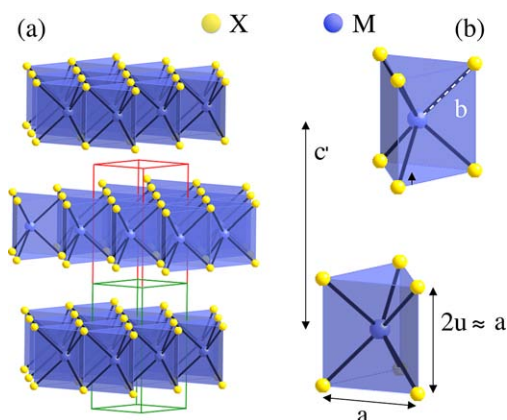

Figure 1 (a) Schematic representation of the atomic structure of MX_2. The bulk compound has a 2H-MX_2 structure with two MX_2 layers per unit cell, each layer being built up from a trigonal prism coordination unit. The small green rectangle represents the unit cell of a monolayer of MX_2, which is doubled (red extension) in the bulk crystal. (b) Detail of the trigonal prisms for the two layers in the bulk compound, showing the lattice constants and the definition of the structural angles used in the text.

Table 1 Lattice parameters used for DFT calculation for MX_2, as taken from Refs. [68–70]. a represents the M-M atomic distance, u the internal vertical distance between the M plane and the X plane, and c' the distance between the M layers. In bulk systems the z-axis lattice parameter is given by $c = 2c'$. All values are in Å units.

	a	u	c'
MoS$_2$	3.160	1.586	6.140
WS$_2$	3.153	1.571	6.160
MoSe$_2$	3.288	1.664	6.451
WSe$_2$	3.260	1.657	6.422

neighbor in-plane $M - M$ and $X - X$ distances, b as the nearest neighbor $M - X$ distance and u as the distance between the M and X planes. The MX_2 crystal forms an almost perfect trigonal prism structure with b and u very close to the their ideal values $b \simeq \sqrt{7/12}a$ and $u \simeq a/2$. The experimental values of these lattice distances of the bulk compounds are given in Table 1 for the four materials investigated [42, 67, 68]. The in-plane Brillouin zone is thus characterized by the high-symmetry points $\Gamma = (0,0)$, K $= 4\pi/3a(1,0)$, and M $= 4\pi/3a(0,\sqrt{3}/2)$.

DFT calculations are done using the SIESTA code [71, 72], with the exchange-correlation potential of Ceperly-Alder [73] as parametrized by Perdew and Zunger [74].
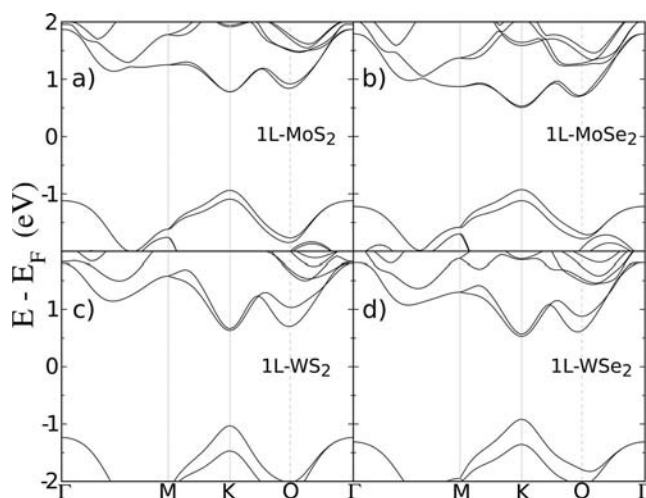
Figure 2 Band structure of single layer MoS_2, $MoSe_2$, WS_2 and WSe_2 obtained from DFT calculations, including SOC. Dashed vertical lines indicate the position of the Q point in the BZ (see text).
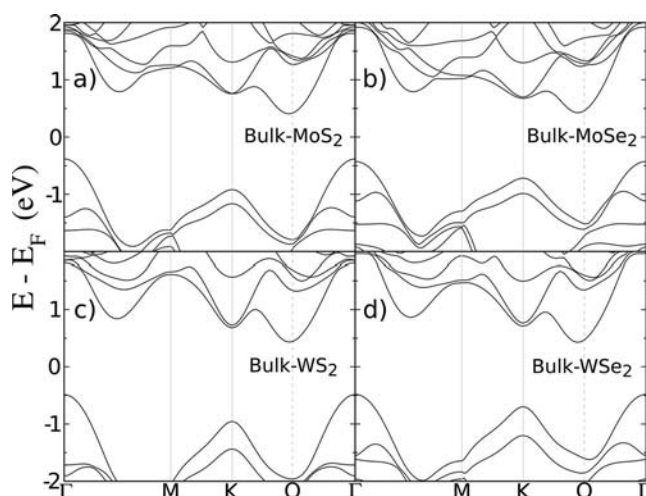

Figure 3 Band structure of bulk MoS_2, $MoSe_2$, WS_2 and WSe_2 obtained from DFT calculations.

Table 2 Band gap and splitting of the valence band (VB) and conduction band (CB) at different points of the BZ obtained from our DFT calculations Figs. 2-3. The gap for monolayer samples is always direct, whereas for bilayer and bulk systems we give the direct/indirect gap for each compound (which values are shown are separated by a hyphen as follows: direct-indirect). All the energies are expressed in eV.

	Bandgap	VB(K)	VB(Γ)	CB(K)	CB(Q)
			Monolayer		
MoS_2	1.715	0.153		0.0041	0.0832
WS_2	1.659	0.439		0.0333	0.339
$MoSe_2$	1.413	0.193		0.0258	0.0
WSe_2	1.444	0.439		0.0396	0.275
			Bilayer		
MoS_2	1.710-1.198	0.181	0.737	0.0	0.457
WS_2	1.658-1.338	0.451	0.677	0.0357	0.528
$MoSe_2$	1.424-1.194	0.213	0.649	0.0253	0.417
WSe_2	1.442-1.299	0.454	0.649	0.0428	0.522
			Bulk		
MoS_2	1.679-0.788	0.245	1.018	0.0	0.874
WS_2	1.636-0.917	0.482	1.426	0.044	0.922
$MoSe_2$	1.393-0.852	0.267	0.695	0.0228	0.819
WSe_2	1.407-0.910	0.504	1.075	0.0548	0.919

We consider also a split-valence double-ζ basis set including polarization functions [75]. The energy cutoff and the Brillouin zone sampling were chosen to converge the total energy with a value of 300 Ry and $30 \times 30 \times 1$ ($30 \times 30 \times 30$) in the case of the monolayer and bilayer (bulk), respectively. The energy cutoff was set to 10^{-6} eV. We account for the spin-orbit interaction of the different compounds following the method developed in Ref. [76] Figs. 2–3 show the obtained band structures for single-layer, bilayer and bulk samples of MX_2. The lattice parameters used in this calculation are given in Table 1. In Table 2 we summarize the most important features of the band structures calculated in this work, like the energy gaps and the splitting of the valence and conduction bands at different points of the BZ. In Tables 3 and 4 we list details of the band structure of different TMDs obtained in other works in the bibliography. A detailed description of the orbital character of the bands can be found in Ref. [7]. The valence and conduction bands are made by hybridization of the d_{xy}, $d_{x^2-y^2}$ and $d_{3z^2-r^2}$ orbitals of the transition metal M, and the p_x, p_y and p_z orbitals of the chalcogen atoms X. All the single-layer compounds shown in Fig. 2 are direct gap semiconductors, with the gap lying at the two inequivalent K points of the hexagonal BZ. The most important orbital contribution at the edge of the valence band at the K point is due to a combination of d_{xy} and $d_{x^2-y^2}$ of the metal M, which hybridize to p_x and p_y orbitals of the chalcogen atoms X. On the other hand, the edge of the conduction band has a main contribution due to $d_{3z^2-r^2}$ of M, plus a minor contribution of p_x and p_y orbitals of X [7].

Review Article

Table 3 Band gap obtained in other works using different methods or functionals as local-density approximation (LDA), generalised gradient approximation (GGA), hybrid functionals as the Heyd-Scuseria-Ernzerhof (HSE) and the GW approximation. Values separated by a hyphen are the direct-indirect gap. All the energies are expressed in eV.

|	LDA	GGA	HSE	GW	Exp
			Monolayer		
MoS$_2$	1.79 [77]/1.89 [68]/1.76 [78]/1.86 [79]	1.60 [47]/1.59 [78]/1.67 [79]	2.05 [47]/2.32 [80]/1.786 [81]/2.25 [79]	2.82 [47]/2.759 [48]/2.41 [82]/2.66 [79]	1.8 [83, 84]/1.90 [8]/1.86 [85]
WS$_2$	2.05 [68]/1.94 [79]	1.56 [47]/1.80 [59]/2.1 [86]/1.9	1.87 [47]?/1.81 [79]	2.88 [47]/2.32 [79]	2.91 [79]
MoSe$_2$	1.58 [68]/1.63 [79]	1.35 [47]/1.44 [59]/1.44 [79]	1.75 [47]/1.99 [79]	2.41 [47]/2.31 [79]	1.76 [87]/1.58 [11]/1.55 [88]
WSe$_2$	1.61 [68]/1.45 [78]/1.74 [79]	1.19 [47]/1.25 [83]/1.32 [37]/1.19 [78]/1.55 [79]	1.68 [47]/2.10 [79]	2.42(Indirect!) [47]/2.51 [79]	1.64 [83]/1.64 [37]
			Bilayer		
MoS$_2$	1.68 [82]/1.75-1.17 [78]	1.275 [89]/1.56-1.17 [78]	1.9 [80]/1.480 [81](Γ to K)	1.888 [48]/2.32 [82]/1.18(Γ to K) [9]	1.88/1.6 [8]/1.51 [9]
WS$_2$	–	1.37 [89]	–	–	1.7 [9]
MoSe$_2$		1.12 [89]			
WSe$_2$	1.35 [68]/1.68-1.27 [78]	1.23 [83]/1.1 [9]/1.41-1.12 [37]/1.19-1.14 [78]	–	–	1.5 [9]/1.59-1.51 [37]
			Bulk		
MoS$_2$	1.67 [82]/0.75 [68]/1.71-0.72 [78]	1.55-0.92 [78]/1.62-0.88 [90]	1.37 [80]/1.328 [81]	1.287 [48]/2.23 [82]/2.07-1.23 [90]	1.8/1.29 [8]/1.23 [91]/1.29 [92]
WS$_2$	0.89 [68]	1.21 [83]/1.65-0.94 [90]	–	2.13-1.30 [90]	1.57 [83]/1.35 [91]
MoSe$_2$	0.80 [68]	1.39-0.84 [90]	–	1.83-1.11 [90]	1.09 [91]/1.1 [92]
WSe$_2$	0.97 [68]	1.5-0.81 [78]/1.33-0.92 [90]	–	1.75-1.19 [90]	1.2 [91]/1.60-1.44 [37]

The main difference between the MoX_2 [Fig. 2(a) and (b)] and WX_2 [Fig. 2(c) and (d)] compounds is observed in the splitting of the valence band for each case, which is due to SOC. Whereas for the Mo compounds it is of the order of ∼150 meV, for the heavier W compounds increases up to ∼400 meV. SOC also lead to a splitting of the conduction band at both, the band edge at the K point [67], as well as at the secondary minimum Q which lies between the Γ and K points of the BZ (indicated in Figs. 2 and 3 by a dashed vertical line). Notice that, since Q is not a high symmetry point of the BZ, the minima of the conduction band for bilayer and bulk materials do not lie exactly at the same point than for single layers. This is why the minima of the conduction band in Figs. 4 and 3 are slightly shifted with respect to the single-layer Q point.

For monolayer samples and around the K and K' points, it is possible to assign a spin projection to the different Bloch states along the normal to the MX_2 plane. It is possible to define a sign for the SOC induced splitting of the band n from the difference $\Delta_n^{SO}(\mathbf{k}) = \varepsilon_{n\uparrow}(\mathbf{k}) - \varepsilon_{n\downarrow}(\mathbf{k})$. Time reversal symmetry implies that $\Delta_n^{SO}(\mathbf{k}) = -\Delta_n^{SO}(-\mathbf{k})$, leading to splitting of opposite sign at the K and K' points. DFT calculations show, for the K point of the conduction band, a negative sign for Δ^{SO} for the Mo compounds (~ -3 meV for MoS$_2$ and ~ -21 meV for MoSe$_2$) and a positive sign for the W compounds (∼27 meV for WS$_2$ and ∼38 meV for WSe$_2$) [67]. Notice that the SOC splitting of the conduction band is larger for the Se compounds as compared to the S compounds. This is expected due to the heavier mass of selenium as compared to sulfur. Since the orbital weight of the p_x and p_y orbitals of chalcogen atoms at the K point of the conduction band is of the order of ∼20% [7], first order processes associated to this X atoms lead to a contribution to the SOC splitting, being more noticeable for the Se compounds. Recent calculations suggest that Coulomb interaction can modify the SOC split bands [93].

Ann. Phys. (Berlin) **526**, No. 9–10 (2014)

annalen
der physik

Review Article

Table 4 Splitting at the valence band at K obtained in other works using different methods or functionals as LDA, GGA, all-electron full-potential linearised augmented-plane wave (FPLAPW), HSE and the GW approximation. All the energies are expressed in eV.

	LDA	GGA	FPLAPW	HSE	GW	Exp
Monolayer						
MoS_2	0.1901 [77]	0.147 [83]/0.146 [47]/0.147 [67]	0.148 [35]	0.193 [47]/0.188 [81]	0.164 [47]/0.146 [48]/0.112 [82]	0.150 [8]/0.170 [47]
WS_2	–	0.435 [83]/0.425 [47]/0.433 [67]	0.426 [35]	0.521 [47]	0.456 [47]	–
$MoSe_2$	–	0.183 [47]/0.186 [67]	0.183 [35]	0.261 [47]	0.26 [47]	0.180 [11]
WSe_2	–	0.461 [47]/0.463 [67]/0.43 [37]	0.456 [35]	0.586 [47]	0.501 [47]	–
Bilayer						
MoS_2	0.1738 [82]	0.17 [89]	–	0.201 [81]	0.174 [48]/0.160 [82]	0.170 [8]
WS_2	–	–	–	–	–	–
$MoSe_2$	–	–	–	–	–	–
WSe_2	–	0.43 [37]	–	–	–	–
Bulk						
MoS_2	0.2201 [82]/0.258 [92]	0.23 [89]	0.184 [81]	0.238 [48]/0.2306 [82]	–	0.180 [8]/0.161 [92]
WS_2	–	–	–	–	–	–
$MoSe_2$	0.294 [92]	–	–	–	0.175 [92]	–
WSe_2	–	–	–	–	–	–
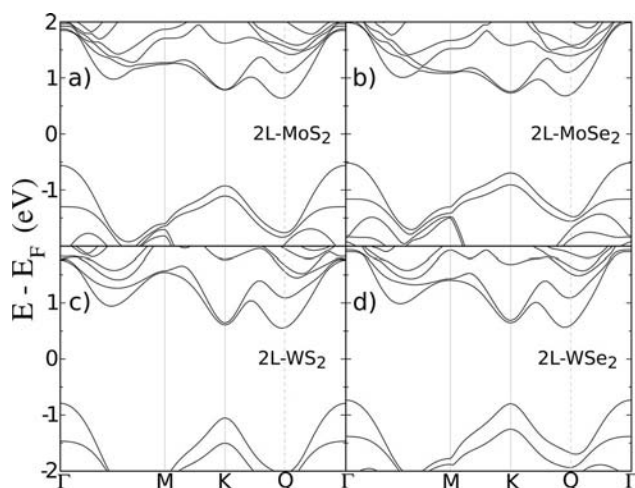
Figure 4 Band structure of bilayer MoS_2, $MoSe_2$, WS_2 and WSe_2 obtained from DFT calculations.

3 Effect of strain

The phonon structure of TMDs considered here is highly sensitive to strain. The Raman spectra of these compounds contain two main peaks which correspond to the A_{1g} out-of-plane mode, where the top and bottom X atoms are moving out of plane in opposite directions while M is fixed, and the E_{2g}^1 in-plane mode where the M and X atoms are moving in-plane in opposite directions [94, 95]. These phonon modes are red shifted with increasing temperatures, which might point the importance of anharmonic contributions to the interatomic potentials [65]. The E_{2g}^1 mode is very sensitive to applied strain. Applying uniaxial strain lifts the degeneracy of this mode, leading to red shifting and splitting into two distinct peaks for strain of just 1% [25, 96, 97]. The particular electronic structure and phonon modes of TMDs suggest that band structure engineering methods can be used for electronic and optoelectronic applications. This technique can be especially useful for TMDs which have been shown to sustain elastically deformations up to 11% without breaking the material [98].

Furthermore, the SOC induces a finite band splitting in single-layer systems also at the six inequivalent valleys at the Q point of the BZ [35, 43], with the corresponding entanglement of spin/valley/orbital degrees of freedom

[99]. At the microscopic level, we remind that the main orbital character of the conduction bands at the Q point is due to a roughly equal distribution of the $d_{x^2-y^2}$ and d_{xy} orbitals of the transition metal M, and of the p_x and p_y orbitals of the chalcogen atom X. The rather large contribution from both p- and d-orbitals leads to a strong hybridization between X and M atoms at this Q point of the BZ. This makes these states highly sensitive to uniform and local strains and lattice distortions [25]. In fact, since the minimum of the conduction band at Q becomes the effective band edge in bilayer and multilayer samples (see Figs. 4 and 3), this suggests that the states at the minima of the conduction band at the Q are good candidates for tuning the spin/orbital/valley entanglement in these materials by means of strain engineering [25] or (in multilayer systems) by means of electric fields [32].

The application of forces across specific axes of the crystal structure induces strain in the sample which, at the same time, can be used to modify the band structure of TMDs. A reduction of the band gap can be achieved under uniaxial compressive strain across the c-axis of the crystal structure of MX_2 [16]. On the other hand, biaxial tensile strain makes the minimum of the conduction band at the Q point to move upward, while the conduction band at the K point moves downward with no significant effect in the valence band at the Γ point. Furthermore, tensile strain is expected to lower the electron effective mass [22] and consequently improve electron mobility, and could also lead to band degeneracy. Some of these theoretical results have been confirmed by strain experiments in single layer and multi-layer MX_2, which shows a change in the band gap up to ~300 meV per 1% applied strain [25, 96, 97]. Strain can be induced by depositing MoS$_2$ on hexagonal boron nitride (h-BN), which can lead to a direct-to-indirect gap transition, as predicted by first-principle calculations [100]. Recent proposals suggest that time-reversal invariant topological phases in TMDs can be engineered by application of strain [101].

Of special interest is the use of strain engineering on MX_2 to create a broad-band optical funnel. This idea, proposed theoretically by Feng *et al.* [13] and confirmed experimentally by Castellanos-Gomez *et al.* [25] consists on continuously change the strain across a sheet of monolayer MoS$_2$, leading to a continuous variation of the optical band gap, which allows not only the capture of photons across a wide range of the solar spectrum, but also guidance of the resulting generated excitons toward contacts.

4 Effect of disorder

Disorder in the lattice structure, such as adatoms or vacancies, can strongly modify the optical and transport properties of materials. In particular the mobility of TMDs is highly dependent on the screening environment and is limited by the presence of impurities in the samples [102–105]. Experimental results show that the optical and transport properties of these materials can be influenced by the existence of defects in their chemical and structural composition. Vacancies in MX_2 crystals trap free charge carriers and localize excitons, leading to new peaks in the photoluminescence spectra [106]. Such vacancies can be created by means of thermal annealing and α-particle [106] or electron beam irradiation [107]. The optical spectrum of bilayer MoS$_2$ presents a broad peak at ~1.77 eV which has been associated to impurities [32], whereas the mobility of multilayer samples has been shown to highly depend on the substrate and dielectric effects [108]. Line defects, which separate patches or islands where the layer direction is opposite to its surrounding, can lead to changes in the carrier mobility [64]. Furthermore, short-range scatterers have been proposed as the main limitation for the mobility of chemical vapor deposition (CVD) grown single-layer MoS$_2$ [56, 57]. Recent scanning tunneling microscopy (STM) and scanning tunneling spectroscopy (STS) in combination with transport measurements suggest that the intrinsic n-doping in bulk MoS$_2$ is due to point defects which are consistent with S vacancies. Moreover, the significantly higher n-doping observed in thin films deposited on SiO$_2$ is extrinsic and has been attributed to trapped donors at the interface with the SiO$_2$ substrate [109]. The controlled creation of defects could be exploited as a route to manipulate the electronic properties of these materials.

On the theoretical ground, the effect of disorder has been first studied using DFT methods [21, 58–61, 63–65]. The study of adsorption of adatoms and creation of vacancy defects in MoS$_2$ nanoribbons have shown that a net magnetic moment can be achieved through the adsorption of Co adatoms to the non-magnetic armchair nanoribbons. Furthermore, apart from the spin-polarization, significant charges can be transferred to (or from) the adatom [58]. Spin-polarized DFT calculations for MoS$_2$ antidots show that the net spin and the stability of spin states can be engineered by controlling the type and distance of internal nanoholes. The case of only S-terminated antidots is found that can exhibit a large net spin above room temperature [63].

Ann. Phys. (Berlin) **526**, No. 9–10 (2014)

annalen
der physik

The electronic and optical properties of single-layers of MoS_2 and WS_2 in the presence of vacancies have been also studied within a *real space* tight-binding (TB) model for large systems, containing millions of atoms, by solving the time-dependent Schrödinger equation, and by means of numerically exact Kubo formula calculations [66]. Vacancies induce states in the middle of the gap whose energy depends on the specific vacant atoms, and the optical transitions involving the impurity bands lead to a background contribution in the optical conductivity at low energies, which has been proposed to be behind the features observed in photoconductivity experiments [8]. MX_2 samples also show a significant asymmetry between electrons and holes [108], such that the DC conductivities and mobilities are larger for holes. When comparing the MS_2 compounds, it is found higher mobilities for p-doped WS_2 than for MoS_2 [66].

5 Spin/valley/layer coupling

In single layers of MX_2, the lack of inversion symmetry as well as the SOC leads to a break in spin degeneracy along both, the valence and conduction bands, and also causes valley Hall effect where carriers flow into opposite transverse edges upon application of an in-plane electric field [29, 33, 110, 111]. In addition, time reversal symmetry of the single layers of MX_2 together with non degeneracy of the spin energy bands lead to a coupling of spin and valley states [31]. This results in valley-dependent optical polarization selection for individual valleys. Since time reversal symmetry forces opposite spin-splitting at each valley, such effect can be used to control the valley polarization by means of optical helicity [27], such that the K valley would correspond to optical selection rules of a certain helicity as well as carriers of a fixed spin, while the K' valley would correspond to opposite conditions. This makes possible to control carrier spin as well as carrier confinement within a specific valley with circularly polarized light, an effect that has been observed experimentally [27, 29, 33]. Since inter-valley scattering is in principle forbidden due to the breaking of spin degeneracy, this suggests long spin lifetimes in single layers of MX_2. As a matter of fact, spin lifetimes larger than 1 ns have been determined experimentally [27], in agreement with theoretical calculations for intravalley SOC mediated spin relaxation in MoS_2 [34]. In the absence of defects, spin relaxation of the carriers is also possible due to flexural deformations of the samples [112].

New interesting features are present in bilayers of MX_2, which consists on a stack of two single layers in-plane rotated by 180° with respect to each other, bound by means of weak van der Waals interactions. The inter-layer hopping of electrons between different layers leads to a strong modification of the band structure, driving a transition from a direct gap semiconductor in single-layer systems to an indirect gap semiconductor in bilayer compounds, as it can be seen by comparing Figs. 2 and 4. The inter-layer hopping, which links mainly the p orbitals of the chalcogen atoms X of different layers [7], lead to a splitting of the maximum of the valence band at the Γ point, which becomes the effective valence band edge, as well as a splitting of the minimum of the conduction band at the Q point, which becomes the absolute minimum of the conduction band [43].

Contrary to single-layer MX_2, bilayer MX_2 presents point-center inversion symmetry [32, 37, 113]. Therefore, the band structure of bilayer MX_2 remains spin degenerate even in the presence of SOC. However, since the SOC does not couple orbitals of different layers, each single band preserves a finite entanglement between spin, valley and the layer index. Such spin-valley-layer coupling can be observed at the K point of the valence band [113], as well as at the conduction band [43]. This last case can be of special interest for slightly electron-doped bilayer MX_2, whose Fermi surface presents six pockets centered at the inequivalent Q valleys of the BZ, and no pockets at the K and K' valleys. Of special interest are the families of TMDs with stronger spin-orbit interaction, like WS_2 and WSe_2, for which the SOC can be larger than the inter-layer hopping, enhancing the spin/layer/valley entanglement. Then, although inversion symmetry forces each Fermi pocket to be spin degenerate, the layer polarization makes that each layer contributes with opposite spin in alternating valleys. This effect can be useful for *valleytronics* devices. The importance of spin and valley states was proven by optical probes in bilayer MoS_2, obtaining a reduction of the photoluminescence by more than 20 times, and hole spin lifetime was 3 orders smaller than those observed in single layers of MoS_2 [27]. The control and tuning of circularly polarized photoluminescence from bilayer MoS_2 can be achieved with the application of a gate voltage, which breaks inversion symmetry due to the electric field, as it has been shown by recent experiments [32].

6 Excitons

The additional *spin-like* quantum numbers discussed in Sec. 5 play an important role in the physics of excitons in TMDs. The reduced dielectric screening in monolayer and few layer samples suggest that strong excitonic

Table 5 Binding energies (in eV) for the neutral excitons obtained from different approaches and from experiments, for monolayer, bilayer and bulk TMDs

	Monolayer		Bilayer	Bulk	
	Effective model	GW	GW	Exp.	GW
MoS_2	0.54 [49]	0.897 [48]/1.03 [47]/1.1 [61]/0.5 [13]/0.54 [22]	0.424 [48]	0.08 [61]	0.13 [61]/0.025 [48]
WS_2	0.47 [49]	0.91 [47]	–	–	–
$MoSe_2$	0.50 [49]	1.04 [47]/0.54 [22]	–	0.07 [61]	0.11 [61]
WSe_2	0.42 [49]	0.90 [47]	–	–	–

effects should appear in these materials. In fact, the existence of highly stable neutral and charged excitons has been proven experimentally [28, 44, 46]. In those experiments, optically excited electrons and holes are bound together by means of Coulomb interaction. Contrary to excitons in conventional semiconductors as GaAs, for which the excitons form at the Γ point of the BZ, excitons in TMDs occur at the K and K' points of the BZ, leading to the so called valley excitons, which open new opportunities to manipulate and control the valley index by means of optical probes, as we have discussed in the previous section. The large SOC splitting of the valence band at the K point leads to two excitonic features in the photo-absorption spectrum [8], usually denoted as the A and B excitons. On the other hand, the binding energy of the charged excitons (usually called *trions*) is unexpectedly large (18 meV for MoS_2 [28], and 30 meV for both $MoSe_2$ [44], and WSe_2 [46]), pointing out that Coulomb interactions are very strong in these families of layered TMDs.

A large exciton binding energy (∼0.32 eV) and a significant deviation from the conventional hydrogenic model, typically used to describe the Wannier excitons in inorganic semiconductors, has been found in the full sequence of excited (Rydberg) exciton states in monolayer and few-layer WS_2, measured by optical reflexion experiments [114]. A theoretical microscopic model that considers the modification of the functional form of the Coulomb interaction due to the nonlocal nature of the effective dielectric screening has been successfully applied to explain these unusually strong electron-hole interactions [114].

To tackle this problem using first principle methods, one needs to go beyond DFT calculations since it is well know that Kohn-Sham energies do not correspond to quasiparticle energies. A better route is to consider *GW* approximation in conjunction with Bethe-Salpeter equation (BSE) to consider the two-particle excitations [47, 48]. Other possibility is to use an effective mass model (parametrized by *ab initio* calculations), and including appropriate screening of the interactions for quasi-2D semiconductors [49]. The separation between the excitons is directly related to the strength of the SOC splitting of the valence band, and excitation energies in the range 1 to 2 eV have been predicted [47], suggesting a potential application of TMDs for optoelectronic devices in the near-IR to the red regime. In Table 5 we list the binding energies of the neutral excitons obtained theoretically from different approximations, as well some experimental values that have been reported in the literature.

7 Superconductivity

Another interesting aspect of the TMDs is the appearance of a superconducting transition with a critical temperature that strongly depends on the carrier density. A superconducting dome, similar to that observed for the layered cuprate, has been experimentally observed in the temperature-carrier density phase diagram of MoS_2 [50, 51], in which the samples were doped by a combination of liquid and solid gating. For the optimal doping $n \sim 1.2 \times 10^{14}$ cm^{-2} the critical temperature is of $T_c \sim 10.8$ K.

Theoretically, the origin of superconductivity in heavily doped MoS_2 was first studied in Ref. [52], by considering the role of both electron-electron and electron-phonon interactions. The estimations for the strength of the different contributions to the effective coupling suggest that superconductivity in MoS_2, under the experimental conditions of Refs. [50, 51], is likely to be induced by the electron-electron interaction. The significant short-range repulsion between carriers at the conduction band allows for a superconducting phase induced by the electron-electron interaction with a nontrivial structure, where the gap acquires opposite signs in the two inequivalent pockets of the conduction

band. On the other hand, DFT calculations for the phase diagram of TMDs suggest that phonon mediated superconductivity is also possible for some range of electron doping, and a charge density wave is also proposed to exist for even higher carrier concentrations [53]. Recently it has been suggested that spin-triplet p-wave superconductivity can be stabilized by Rashba SOC in MoS_2 [54]. Finally, the superconducting proximity effect and the Andreev reflection in MX_2 superconducting-normal (S/N) hybrid junction with n- (p-)doped S and p-doped N regions has been investigated in Ref. [55], finding that the strong SOC enhances the Andreev conductance of the MoS_2-based S/N structure relative to its value in the corresponding structure with gapped graphene.

8 Conclusions

In conclusion, we have discussed the electronic properties of semiconducting TMDs MX_2, where M = Mo, W and X = S, Se. DFT band structure calculations, including the effect of SOC, have been used to discuss the differences between the single layer, bilayer and bulk compounds. The splitting of the bands due to SOC has been discussed in the whole BZ, analyzing the role of the transition metal and the chalcogen atoms at each relevant point of the band structure. We have further reviewed the effect of strain in the samples, discussing how strain engineering is a good route to manipulate and tune the electronic and optical properties of those compounds. Disorder and imperfections in the lattice structure lead to the creation of impurity states in the middle of the gap, which contribute to the photoconductivity. Finally, we have discussed the superconducting phase which has been also experimentally observed in the TMDs, and which present a superconducting dome in the temperature-carrier density phase diagram, which resembles to that of the cuprate superconductors. The different mechanisms proposed to explain the superconducting pairing have been reviewed.

References

[1] A. H. Castro-Neto, F. Guinea, N. M. R. Peres, K. S. Novoselov, and A. K. Geim, Rev. Mod. Phys. **81**, 109 (2009).

[2] L. Britnell, R. Gorbachev, R. Jalil, B. Belle, F. Schedin, A. Mishchenko, T. Georgiou, M. Katsnelson, L. Eaves, S. Morozov et al., Science **335**, 947 (2012).

[3] K. S. Novoselov, D. Jiang, F. Schedin, T. J. Booth, V. V. Khotkevich, S. V. Morozov, and A. K. Geim, Proc. Natl. Acad. Sci. USA **102**, 10451 (2005).

[4] Q. H. Wang, K. Kalantar-Zadeh, A. Kis, J. N. Coleman, and M. S. Strano, Nature Nanotech. **7**, 699 (2012).

[5] D. Jariwala, V. K. Sangwan, L. J. Lauhon, T. J. Marks, and M. C. Hersam, ACS Nano **8**, 1102 (2014).

[6] R. Ganatra and Q. Zhang, ACS Nano **8**, 4074 (2014).

[7] E. Cappelluti, R. Roldán, J. A. Silva-Guillén, P. Ordejón, and F. Guinea, Phys. Rev. B **88**, 075409 (2013).

[8] K. F. Mak, C. Lee, J. Hone, J. Shan, and T. F. Heinz, Phys. Rev. Lett. **105**, 136805 (2010).

[9] W. Zhao, R. M. Ribeiro, M. Toh, A. Carvalho, C. Kloc, A. H. Castro Neto, and G. Eda, Nano Lett. **13**, 5627 (2013).

[10] W. Jin, P.-C. Yeh, N. Zaki, D. Zhang, J. T. Sadowski, A. Al-Mahboob, A. M. van der Zande, D. A. Chenet, J. I. Dadap, I. P. Herman et al., Phys. Rev. Lett. **111**, 106801 (2013).

[11] Y. Zhang, T.-R. Chang, B. Zhou, Y.-T. Cui, H. Yan, Z. Liu, F. Schmitt, J. Lee, R. Moore, Y. Chen et al., Nature Nanotech. **9**, 111 (2014).

[12] A. Castellanos-Gomez, E. Cappelluti, R. Roldán, N. Agraït, F. Guinea, and G. Rubio-Bollinger, Adv. Mat. **25**, 899 (2013).

[13] J. Feng, X. Qian, C.-W. Huang, and J. Li, Nature Photon. **6**, 866 (2012).

[14] P. Lu, X. Wu, W. Guo, and X. C. Zeng, Phys. Chem. Chem. Phys. **14**, 13035 (2012).

[15] H. Pan and Y.-W. Zhang, J. Phys. Chem. C **116**, 11752 (2012).

[16] H. Peelaers and C. G. Van de Walle, Phys. Rev. B **86**, 241401 (2012).

[17] E. Scalise, M. Houssa, G. Pourtois, V. Afanasev, and A. Stesmans, Physica E: Low-dimensional Systems and Nanostructures **56**, 416 (2014).

[18] E. Scalise, M. Houssa, G. Pourtois, V. AfanasŌev, and A. Stesmans, Nano Res. **5**, 43 (2012).

[19] W. S. Yun, S. Han, S. C. Hong, I. G. Kim, and J. Lee, Phys. Rev. B **85**, 033305 (2012).

[20] Y. Li, Y.-L. Li, C. M. Araujo, W. Luo, and R. Ahuja, Catal. Sci. Technol. **3**, 2214 (2013).

[21] M. Ghorbani-Asl, S. Borini, A. Kuc, and T. Heine, Phys. Rev. B **87**, 235434 (2013).

[22] H. Shi, H. Pan, Y.-W. Zhang, and B. I. Yakobson, Phys. Rev. B **87**, 155304 (2013).

[23] L. Hromadová, R. Martoňák, and E. Tosatti, Phys. Rev. B **87**, 144105 (2013).

[24] S. Horzum, H. Sahin, S. Cahangirov, P. Cudazzo, A. Rubio, T. Serin, and F. M. Peeters, Phys. Rev. B **87**, 125415 (2013).

[25] A. Castellanos-Gomez, R. Roldán, E. Cappelluti, M. Buscema, F. Guinea, H. S. J. van der Zant, and G. A. Steele, Nano Lett. **13**, 5361 (2013).

[26] X. Xu, W. Yao, D. Xiao, and T. F. Heinz, Nature Phys. **10**, 343 (2014).

[27] K. F. Mak, K. He, J. Sahn, and T. F. Heinz, Nature Nanotech. **7**, 494 (2012).

[28] K. F. Mak, K. He, C. Lee, G. H. Lee, J. Hone, T. F. Heinz, and J. Shan, Nature Mat. **12**, 207 (2013).

[29] T. Cao, G. Wang, W. Han, H. Ye, C. Zhu, J. Shi, Q. Niu, P. Tan, E. Wang, B. Liu et al., Nat. Commun. **3**, 887 (2012).

[30] G. Sallen, L. Bouet, X. Marie, G. Wang, C. R. Zhu, W. P. Han, Y. Lu, P. H. Tan, T. Amand, B. L. Liu et al., Phys. Rev. B **86**, 081301 (2012).

[31] D. Xiao, G.-B. Liu, W. Feng, X. Xu, and W. Yao, Phys. Rev. Lett. **108**, 196802 (2012).

[32] S. Wu, J. S. Ross, G.-B. Liu, G. Aivazian, A. Jones, Z. Fei, W. Zhu, D. Xiao, W. Yao, D. Cobden et al., Nature Phys. **9**, 149 (2013).

[33] H. Zeng, J. Dai, W. Yao, D. Xiao, and X. Cui, Nature Nanotech. **7**, 490 (2012).

[34] H. Ochoa and R. Roldán, Phys. Rev. B **87**, 245421 (2013).

[35] Z. Y. Zhu, Y. C. Cheng, and U. Schwingenschlögl, Phys. Rev. B **84**, 153402 (2011).

[36] Q. Wang, S. Ge, X. Li, J. Qiu, Y. Ji, J. Feng, and D. Sun, ACS Nano **7**, 11087 (2013).

[37] H. Zeng, G.-B. Liu, J. Dai, Y. Yan, B. Zhu, R. He, L. Xie, S. Xu, X. Chen, W. Yao et al., Sci. Rep. **3**, 1608 (2013).

[38] W. Feng, Y. Yao, W. Zhu, J. Zhou, W. Yao, and D. Xiao, Phys. Rev. B **86**, 165108 (2012).

[39] W.-Y. Shan, H.-Z. Lu, and D. Xiao, Phys. Rev. B **88**, 125301 (2013).

[40] H. Rostami, A. G. Moghaddam, and R. Asgari, Phys. Rev. B **88**, 085440 (2013).

[41] F. Rose, M. O. Goerbig, and F. Piéchon, Phys. Rev. B **88**, 125438 (2013).

[42] G.-B. Liu, W.-Y. Shan, Y. Yao, W. Yao, and D. Xiao, Phys. Rev. B **88**, 085433 (2013).

[43] R. Roldán, M. López-Sancho, E. Cappelluti, J. Silva-Guillén, P. Ordejón, and F. Guinea, arXiv preprint arXiv:1401.5009 (2014).

[44] J. S. Ross, S. Wu, H. Yu, N. J. Ghimire, A. M. Jones, G. Aivazian, J. Yan, D. G. Mandrus, D. Xiao, W. Yao et al., Nature Commun. **4**, 1474 (2013).

[45] C.-C. Wu, D. Jariwala, V. K. Sangwan, T. J. Marks, M. C. Hersam, and L. J. Lauhon, J. Phys. Chem. Lett. **4**, 2508 (2013).

[46] A. M. Jones, H. Yu, N. J. Ghimire, S. Wu, G. Aivazian, J. S. Ross, B. Zhao, J. Yan, D. G. Mandrus, D. Xiao et al., Nature Nanotech. **8**, 634 (2013).

[47] A. Ramasubramaniam, Phys. Rev. B **86**, 115409 (2012).

[48] T. Cheiwchanchamnangij and W. R. L. Lambrecht, Phys. Rev. B **85**, 205302 (2012).

[49] T. C. Berkelbach, M. S. Hybertsen, and D. R. Reichman, Phys. Rev. B **88**, 045318 (2013).

[50] K. Taniguchi, A. Matsumoto, H. Shimotani, and H. Takagi, Appl. Phys. Lett. **101**, 042603 (2012).

[51] J. T. Ye, Y. J. Zhang, R. Akashi, M. S. Bahramy, R. Arita, and Y. Iwasa, Science **338**, 1193 (2012).

[52] R. Roldán, E. Cappelluti, and F. Guinea, Phys. Rev. B **88**, 054515 (2013).

[53] M. Rösner, S. Haas, and T. O. Wehling, ArXiv e-prints (2014), 1404.4295.

[54] N. F. Q. Yuan, K. F. Mak, and K. T. Law, ArXiv e-prints (2014), 1405.3519.

[55] L. Majidi, H. Rostami, and R. Asgari, Phys. Rev. B **89**, 045413 (2014).

[56] W. Zhu, T. Low, Y.-H. Lee, H. Wang, D. B. Farmer, J. Kong, F. Xia, and P. Avouris, Nat. Commun. **5**, 3087 (2014).

[57] H. Schmidt, S. Wang, L. Chu, M. Toh, R. Kumar, W. Zhao, A. H. Castro Neto, J. Martin, S. Adam, B. Oezyilmaz et al., ArXiv e-prints (2014), 1401.1063.

[58] C. Ataca and S. Ciraci, J. Phys. Chem. C **115**, 13303 (2011).

[59] Y. Ma, Y. Dai, M. Guo, C. Niu, J. Lu, and B. Huang, Phys. Chem. Chem. Phys. **13**, 15546 (2011).

[60] J.-w. Wei, Z.-w. Ma, H. Zeng, Z.-y. Wang, Q. Wei, and P. Peng, AIP Advances **2**, 042141 (2012).

[61] H.-P. Komsa and A. V. Krasheninnikov, Phys. Rev. B **86**, 241201 (2012).

[62] M. Ghorbani-Asl, A. N. Enyashin, A. Kuc, G. Seifert, and T. Heine, Phys. Rev. B **88**, 245440 (2013b).

[63] Y. Zhou, P. Yang, H. Zu, F. Gao, and X. Zu, Phys. Chem. Chem. Phys. **15**, 10385 (2013).

[64] A. N. Enyashin, M. Bar-Sadan, L. Houben, and G. Seifert, J. Phys. Chem. C **117**, 10842 (2013).

[65] N. A. Lanzillo, A. Glen Birdwell, M. Amani, F. J. Crowne, P. B. Shah, S. Najmaei, Z. Liu, P. M. Ajayan, J. Lou, M. Dubey et al., Appl. Phys. Lett. **103**, eid093102 (2013).

[66] S. Yuan, R. Roldán, M. I. Katsnelson, and F. Guinea, Phys. Rev. B **90**, 041402 (2014).

[67] K. Kośmider, J. W. González, and J. Fernández-Rossier, Phys. Rev. B **88**, 245436 (2013).

[68] A. Kumar and P. Ahluwalia, Eur. Phys. J. B **85**, 1 (2012).

[69] R. A. Bromley, R. B. Murray, and A. D. Yoffe, J. Phys. C: Solid State Phys. **5**, 759 (1972).

[70] W. Schutte, J. Boer, and F. Jellinek, J. Solid State Chem. **70**, 207 (1987).

[71] J. Soler, E. Artacho, J. Gale, A. García, J. Junquera, P. Ordejón, and D. Sánchez-Portal, J. Phys.: Condens. Matter **14**, 2745 (2002).

[72] E. Artacho, E. Anglada, O. Dieguez, J. Gale, A. García, J. Junquera, R. Martin, P. Ordejón, J. M. Pruneda, D. Sánchez-Portal et al., J. Phys.: Condens. Matter **20**, 064208 (2008).

[73] D. Ceperley and B. J. Alder, Phys. Rev. Lett. **45**, 566 (1980).

Review Article

[74] P. Perdew and A. Zunger, Phys. Rev. B **23**, 5048 (1981).

[75] E. Artacho, D. Sánchez-Portal, P. Ordejón, A. García, and J. Soler, Physica Status Solidi B Basic Research **215**, 809 (1999).

[76] L. Fernández-Seivane, M. Oliveira, S. Sanvito, and J. Ferrer, J. Phys.: Condens. Matter **18**, 7999 (2006).

[77] E. S. Kadantsev and P. Hawrylak, Solid State Commun. **152**, 909 (2012).

[78] W. Huang, X. Luo, C. K. Gan, S. Y. Quek, and G. Liang, Phys. Chem. Chem. Phys. **16**, 10866 (2014a).

[79] Y. Ding, Y. Wang, J. Ni, L. Shi, S. Shi, and W. Tang, Physica B: Condensed Matter **406**, 2254 (2011).

[80] J. K. Ellis, M. J. Lucero, and G. E. Scuseria, Appl. Phys. Lett. **99**, 261908 (2011).

[81] F. Zahid, L. Liu, Y. Zhu, J. Wang, and H. Guo, AIP Advances **3**, 052111 (2013).

[82] A. Molina-Sánchez, D. Sangalli, K. Hummer, A. Marini, and L. Wirtz, Phys. Rev. B **88**, 045412 (2013).

[83] H. Sahin, S. Tongay, S. Horzum, W. Fan, J. Zhou, J. Li, J. Wu, and F. M. Peeters, Phys. Rev. B **87**, 165409 (2013).

[84] A. Splendiani, L. Sun, Y. Zhang, T. Li, J. Kim, C.-Y. Chim, G. Galli, and F. Wang, Nano Lett. **10**, 1271 (2010).

[85] T. Eknapakul, P. D. C. King, M. Asakawa, P. Buaphet, R.-H. He, S.-K. Mo, H. Takagi, K. M. Shen, F. Baumberger, T. Sasagawa et al., Nano Lett. **14**, 1312 (2014).

[86] A. Kuc, N. Zibouche, and T. F. Heinz, Phys. Rev. B **83**, 245213 (2011).

[87] S. Lebègue and O. Eriksson, Phys. Rev. B **79**, 115409 (2009).

[88] S. Tongay, J. Zhou, C. Ataca, K. Lo, T. S. Matthews, J. Li, J. C. Grossman, and J. Wu, Nano Lett. **12**, 5576 (2012).

[89] A. Ramasubramaniam, D. Naveh, and E. Towe, Phys. Rev. B **84**, 205325 (2011).

[90] H. Jiang, J. Phys. Chem. C **116**, 7664 (2012).

[91] K. K. Kam and B. A. Parkinson, J. Phys. Chem. **86**, 463 (1982).

[92] T. Böker, R. Severin, A. Müller, C. Janowitz, R. Manzke, D. Voß, P. Krüger, A. Mazur, and J. Pollmann, Phys. Rev. B **64**, 235305 (2001).

[93] Y. Ferreiros and A. Cortijo (2014), arXiv:1403.5283.

[94] A. Molina-Sánchez and L. Wirtz, Phys. Rev. B **84**, 155413 (2011).

[95] C. Lee, H. Yan, L. E. Brus, T. F. Heinz, J. Hone, and S. Ryu, ACS Nano **4**, 2695 (2010).

[96] H. J. Conley, B. Wang, J. I. Ziegler, R. F. Haglund, S. T. Pantelides, and K. I. Bolotin, Nano Lett. **13**, 3626 (2013).

[97] Y. Y. Hui, X. Liu, W. Jie, N. Y. Chan, J. Hao, Y.-T. Hsu, L.-J. Li, W. Guo, and S. P. Lau, ACS Nano **7**, 7126 (2013).

[98] A. Castellanos-Gómez, M. Poot, G. A. Steele, H. S. J. van der Zant, N. Agraït, and G. Rubio-Bollinger, Adv. Mater. **24**, 772 (2012).

[99] H. Yuan, X. Wang, B. Lian, H. Zhang, X. Fang, B. Shen, G. Xu, Y. Xu, S.-C. Zhang, H. Y. Hwang et al., ArXiv e-prints (2014), 1403.2696.

[100] Z. Huang, C. He, X. Qi, H. Yang, W. Liu, X. Wei, X. Peng, and J. Zhong, Journal of Physics D: Appl. Phys. **47**, 075301 (2014b).

[101] M. A. Cazalilla, H. Ochoa, and F. Guinea, Phys. Rev. Lett. **113**, 077201 (2014).

[102] K. Kaasbjerg, K. S. Thygesen, and K. W. Jacobsen, Phys. Rev. B **85**, 115317 (2012).

[103] D. Jariwala, V. K. Sangwan, D. J. Late, J. E. Johns, V. P. Dravid, T. J. Marks, L. J. Lauhon, and M. C. Hersam, Appl. Phys. Lett. **102**, 173107 (2013).

[104] V. K. Sangwan, H. N. Arnold, D. Jariwala, T. J. Marks, L. J. Lauhon, and M. C. Hersam, Nano Lett. **13**, 4351 (2013).

[105] K. Kaasbjerg, K. S. Thygesen, and A.-P. Jauho, Phys. Rev. B **87**, 235312 (2013).

[106] S. Tongay, J. Suh, C. Ataca, W. Fan, A. Luce, J. S. Kang, J. Liu, C. Ko, R. Raghunathanan, J. Zhou et al., Sci. Rep. **3** (2013).

[107] W. Zhou, X. Zou, S. Najmaei, Z. Liu, Y. Shi, J. Kong, J. Lou, P. M. Ajayan, B. I. Yakobson, and J.-C. Idrobo, Nano Lett. **13**, 2615 (2013).

[108] W. Bao, X. Cai, D. Kim, K. Sridhara, and M. S. Fuhrer, Appl. Phys. Lett. **102**, 042104 (2013).

[109] C.-P. Lu, G. Li, J. Mao, L.-M. Wang, and E. Y. Andrei, ArXiv e-prints (2014), 1405.2367.

[110] H.-Z. Lu, W. Yao, D. Xiao, and S.-Q. Shen, Phys. Rev. Lett. **110**, 016806 (2013).

[111] K. F. Mak, K. L. McGill, J. Park, and P. L. McEuen (2014), arXiv:1403.5039.

[112] H. Ochoa, F. Guinea, and V. I. Fal'ko, Phys. Rev. B **88**, 195417 (2013).

[113] Z. Gong, G.-B. Liu, H. Yu, D. Xiao, X. Cui, X. Xu, and W. Yao, Nat. Commun. **4**, 2053 (2013).

[114] A. Chernikov, T. C. Berkelbach, H. M. Hill, A. Rigosi, Y. Li, O. B. Aslan, D. R. Reichman, M. S. Hybertsen, and T. F. Heinz, Phys. Rev. Lett. **113**, 076802 (2014).